

# **1 Snowmelt-driven shifts of a range-expanding plant in**

## **2 alpine ecosystems revealed by ground-based time-lapse**

### **3 cameras**

<sup>4</sup> *Keywords:* alpine vegetation, habitat suitability modeling, climate change

\*Corresponding author

5     **Abstract**

6     *Aim*

7     Climate change is reorganizing alpine vegetation worldwide. However, the  
8     processes linking snow dynamics to fine-scale vegetation redistribution remain  
9     poorly quantified. We ask whether spatial variation in snowmelt timing can  
10    explain and predict the expansion of competitively dominant plants in alpine  
11    landscapes.

12    *Location*

13    Northern Japanese Alps.

14    *Methods*

15    We combined ground-based time-lapse camera observations with habitat suit-  
16    ability models (HSMs) to reconstruct past and project future distributions of  
17    dwarf bamboo (*Sasa* spp.) at 1-meter spatial resolution. Time-lapse images  
18    collected from 2012 to 2021 were used to generate automated vegetation maps  
19    and pixel-level estimates of snowmelt timing. These variables were incorporated  
20    as predictors in the models.

21    *Results*

22    Between 2012 and 2021, *Sasa* cover increased by 48%. Over the same period,  
23    snowmelt timing advanced by an average of 8.6 days per decade. Variable-  
24    importance analyses identified snowmelt day of year (DOY) and distance from  
25    the prior *Sasa* distribution as the strongest determinants of current patterns. This  
26    indicates that both climatic forcing and dispersal constraints shape distributional  
27    change. Scenario-based projections under continued snowmelt advance suggested  
28    further expansion of *Sasa* by 2030.

29    *Main conclusions*

30    Our results demonstrate that snowmelt timing is a key biogeographic driver  
31    structuring the spatial redistribution of dominant alpine plants. They also show  
32    that fine-scale snow–vegetation relationships can be quantified and projected us-  
33    ing ground-based observations. By linking climate-driven processes to vegetation  
34    patterns at meter resolution, this study advances understanding of how alpine  
35    plant distributions respond to changing cryospheric conditions. The approach  
36    provides a transferable basis for assessing climate-induced vegetation reorga-  
37    nization in snow-dominated ecosystems, with direct relevance for conservation  
38    planning.

39     **1. Introduction**

40     Alpine ecosystems are among the most vulnerable to climate change ([Hock et al. \(2019\)](#)). Across mountain regions worldwide, climate-driven shifts in vegetation  
41     have been documented ([Gottfried et al. \(2012\)](#)), including changes in timberline  
42     positions and the spatial reorganization of alpine plant communities. Such shifts  
43     reflect biogeographic responses to environmental gradients and vary regionally  
44     depending on geological context, species interactions, and disturbance regimes  
45     ([Grabherr et al. \(2010\)](#), [Klanderud \(2005\)](#)).

46     A key mechanism underlying these biogeographic shifts is the emergence or  
47     expansion of competitively dominant species, which can rapidly reorganize  
48     community composition by excluding subordinate taxa. For example, grass-  
49     dominated snowbed communities ([Grabherr \(2003\)](#)) and shrub encroachment  
50     into alpine grasslands ([Dullinger et al. \(2003\)](#)) illustrate how dominance hierar-  
51     chies mediate vegetation change across alpine landscapes. In Japanese alpine  
52     ecosystems, dwarf bamboo (*Sasa* spp., hereafter *Sasa*) represents a pronounced  
53     example of such dominance. Earlier snowmelt associated with climate change  
54     promotes *Sasa* invasion into snowbed communities, resulting in substantial re-  
55     ductions in plant species richness ([Kudo et al. \(2011\)](#)). Conversely, vegetation  
56     recovery following *Sasa* removal has been documented ([Kudo et al. \(2017\)](#)), high-  
57     lighting the importance of understanding how climate-driven processes regulate  
58     the spatial dynamics of dominant alpine plants for conservation.

59     Despite their importance, fine-scale biogeographic processes in alpine ecosystems  
60     remain difficult to quantify. Alpine regions are remote and topographically  
61     rugged, making traditional vegetation surveys costly and logistically demanding.  
62     Satellite-based observations are also limited by frequent cloud cover and the  
63     fine-grained, mosaic structure of alpine vegetation. These constraints hinder  
64     our ability to link environmental drivers, such as snowmelt timing, to observed  
65     vegetation patterns at ecologically meaningful scales.

66     To address these challenges, a method for generating high-resolution vegetation  
67     classification maps using ground-based time-lapse cameras has been developed  
68     ([Okamoto et al. \(2024\)](#)). This approach exploits temporal changes in vegetation  
69     colour captured by fixed cameras and applies precise georectification to align  
70     ground-based imagery spatially. By combining high temporal frequency with fine  
71     spatial resolution, time-lapse cameras provide an opportunity to quantify climate-  
72     driven biogeographic processes that are difficult to observe using conventional  
73     approaches.

74     Here, we apply this framework to a Japanese alpine system as a model case to  
75     examine snowmelt-driven vegetation dynamics. Specifically, we quantified *Sasa*  
76     expansion into alpine meadows on the western slope of Mt. Tateyama in the  
77     northern Japanese Alps. In the nearby Murodo-daira plateau, *Sasa* species (*Sasa*  
78     *kurilensis*, *Sasa spiculosa*, *Sasa senanensis*, and *Sasa palmata*) expanded by  
79     44–260% between 1977 and 2015 ([Yoshida et al. \(2016\)](#)). Previous studies relied  
80     primarily on field surveys or manual interpretation of aerial photographs, limiting

82 spatial resolution and temporal continuity. By contrast, automated processing  
83 of time-lapse imagery enabled us to generate large-scale, high-resolution maps of  
84 *Sasa* distribution across the study area.

85 A particular advantage of time-lapse cameras is their capacity to capture  
86 frequent, site-specific records of snowmelt timing, a fundamental driver of alpine  
87 vegetation dynamics. Leveraging this capability, we modelled *Sasa* distributions  
88 derived from time-lapse imagery using environmental variables such as snowmelt  
89 timing and topographic factors, and predicted distributional shifts under scenarios  
90 of earlier snowmelt. Habitat suitability models (HSMs)—statistical frameworks  
91 relating species occurrence to environmental conditions—are widely used to  
92 elucidate habitat preferences ([Guisan et al. \(1998\)](#)), inform conservation planning  
93 ([Larson et al. \(2004\)](#), [Xue et al. \(2021\)](#)), forecast biological invasions ([Gallien  
et al. \(2010\)](#), [Gallien et al. \(2012\)](#)), and assess range shifts and extinction risks  
95 under climate change ([Thomas et al. \(2004\)](#), [Bakkenes et al. \(2002\)](#), [Amagai  
et al. \(2022\)](#)).

97 Using HSMs constructed from observed *Sasa* distributions and their temporal  
98 changes, we addressed two primary questions: (1) whether snowmelt timing acts  
99 as a critical determinant of dominant plant distributions in alpine landscapes,  
100 and (2) how such distributions may shift under future conditions of earlier  
101 snowmelt. By linking high-resolution observations with predictive modelling,  
102 this study demonstrates how ground-based time-lapse imagery can be used to  
103 detect and forecast climate-driven vegetation redistribution, with implications  
104 for conservation monitoring and management in alpine ecosystems.

## 105 2. Materials and Methods

106 Although demonstrated in a Japanese alpine system, the workflow presented  
107 here is applicable to any snow-dominated ecosystem monitored by fixed ground-  
108 based cameras, including existing alpine webcam networks such as those estab-  
109 lished in the Swiss Alps ([Portenier et al. \(2020\)](#)). The approach is designed  
110 as a biogeographic inference pipeline that links climate-driven processes, rep-  
111 resented by snowmelt timing, to vegetation patterns and their redistribution  
112 under environmental change.

113 Figure 1 presents an overview of the workflow. Using time-lapse imagery  
114 from the northern Japanese Alps, we quantified *Sasa* expansion and measured  
115 the snowmelt day of year (DOY). *Sasa* expansion was assessed by comparing  
116 vegetation classification maps derived from imagery captured in 2012 and 2021,  
117 while snowmelt DOY was determined from imagery spanning 2011–2021. Based  
118 on the resulting *Sasa* distribution and its changes, together with snowmelt DOY  
119 and topographic features derived from a digital elevation model (DEM), we  
120 constructed habitat suitability models (HSMs) to predict *Sasa* distribution and  
121 expansion. Finally, we incorporated future snowmelt DOY projected from our  
122 observations into the HSMs to generate detailed forecasts of future *Sasa* invasion.

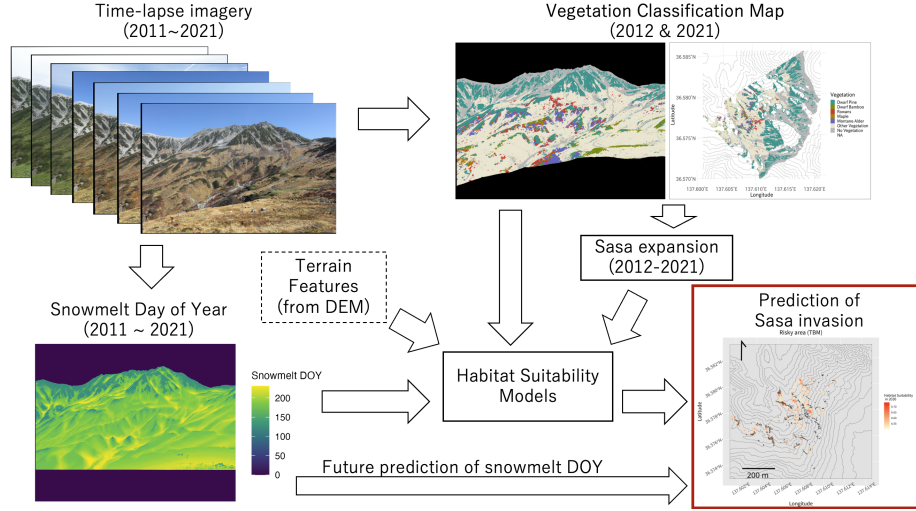


Figure 1: Overview of the proposed method.  
We used time-lapse imagery and a DEM for constructing HSMs for predicting the *Sasa* distribution.

### 123 2.1. Image acquisition

124 To monitor the distribution of *Sasa*, we used images captured by a digital  
 125 time-lapse camera (EOS 5D MK2, Canon Inc., 21 megapixels) installed by the  
 126 National Institute for Environmental Studies on the Murodo-sanso mountain  
 127 lodge (approximately 2,450 m a.s.l.) in the northern Japanese Alps. Since  
 128 2010, the camera has documented snowmelt and vegetation dynamics on the  
 129 western slope of Mt. Tateyama (2,350–3,015 m), taking photographs hourly from  
 130 6:00 to 19:00 between April and November. For details of the installation and  
 131 operation, see [Okamoto et al. \(2024\)](#). In this study, we used images taken in  
 132 September–October of 2012 and 2021 for quantifying *Sasa* expansion.

133 A major advantage of time-lapse cameras is their ability to capture fine-scale,  
 134 daily changes in snow cover. Frequent cloud cover and the steep topography  
 135 of alpine regions often hinder continuous satellite observations, making ground-  
 136 based time-lapse imagery particularly valuable. Because earlier snowmelt is con-  
 137 sidered a primary driver of *Sasa* expansion ([Kudo et al. \(2011\)](#)), high-frequency  
 138 and high-resolution data on snowmelt timing are essential for understanding and  
 139 predicting its spread. Therefore, we also used imagery acquired from April to  
 140 August between 2011 and 2021 to calculate the snowmelt day of year (DOY) for  
 141 each pixel. Snowmelt detection followed a workflow based on Otsu's binarization  
 142 method ([Otsu \(1979\)](#)) as described in [Ide and Oguma \(2013\)](#). The extracted  
 143 snowmelt DOYs were subsequently incorporated into the habitat suitability  
 144 models (HSMs).

145      *2.2. Automated production of vegetation classification maps*

146      Vegetation classification maps were produced using the method developed by  
147      Okamoto et al. (2024), which consists of three main steps: image alignment,  
148      vegetation classification, and automated georectification.

- 149      • **Image alignment:** All images from 2012 and 2021 were aligned to  
150      enable precise temporal comparisons. Following Okamoto et al. (2024), we  
151      applied a local-feature-based automated alignment approach.
- 152      • **Vegetation classification:** Temporal changes in leaf color during  
153      autumn were analyzed using a recurrent neural network (RNN), which  
154      classified each pixel into seven categories: Dwarf Pine (*Pinus pumila*),  
155      Dwarf Bamboo (*Sasa* spp.), Rowans (*Sorbus sambucifolia*, *S. matsumurae*),  
156      Maple (*Acer tschonoskii*), Montane Alder (*Alnus viridis* subsp.  
157      *maximowiczii*), Other Vegetation (alpine shrubs and herbaceous plants),  
158      and No Vegetation.
- 159      • **Automated georectification:** We automatically extracted ground  
160      control points (GCPs) from existing orthorectified aerial photographs and a  
161      digital elevation model (DEM), estimated camera parameters (orientation,  
162      focal length, and lens distortion), and transformed the images into georeferenced  
163      data at 1 m spatial resolution using the Python package `alproj`  
164      (<https://github.com/Okam/alproj>). The aerial photographs and DEM used  
165      for georectification were identical to those in Okamoto et al. (2024).

166      *2.3. Quantification of Sasa expansion*

167      To detect nine-year changes in *Sasa* distribution, we overlaid vegetation classification  
168      maps from 2012 and 2021 (Figure 2). We calculated the area occupied by  
169      *Sasa* in each year and quantified its expansion by comparing the two classification  
170      maps. Because *Sasa* can remain beneath shrub canopies, shrub encroachment  
171      and growth may cause *Sasa* to become undetectable in time-lapse imagery. Consequently,  
172      areas that appear to have decreased in *Sasa* cover may not represent  
173      true declines. To avoid underestimating expansion due to this limitation, we  
174      defined the primary expansion metric as the area of transitions from non-*Sasa*  
175      to *Sasa* (i.e., expansion area).

176      *2.4. Habitat suitability modeling*

177      To predict future *Sasa* expansion and understand its driver, we constructed  
178      habitat suitability models (HSMs). *Sasa* forms complex rhizome systems and  
179      extensive clonal networks (Suyama et al. (2000)). While its expansion primarily  
180      occurs through rhizome elongation, seed dispersal can also take place after mass  
181      or partial flowering events (Miyazaki et al. (2009); Mizuki et al. (2014); Kudo  
182      et al. (2011)). As a result, *Sasa* can potentially expand both gradually through  
183      rhizome growth and over longer distances through seed dispersal.

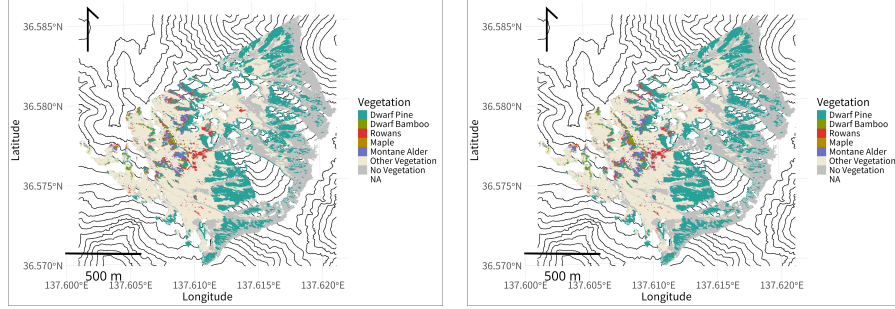


Figure 2: Vegetation classification results for 2012 and 2021.  
Vegetation classification maps for 2012 (left) and 2021 (right). *Sasa* expansion was quantified by comparing the spatial extent of its distribution between the two maps.

To capture these contrasting dispersal processes, we developed two complementary models that predict the *Sasa* distribution observed in 2021 from environmental conditions and the baseline distribution in 2012. The **Topography-Based Model (TBM)** incorporates only topographic variables such as elevation, slope, and snowmelt DOY, representing potential expansion areas assuming that *Sasa* can disperse freely via seeds. In contrast, the **Topography–Distance Model (TDM)** additionally includes the distance from the 2012 *Sasa* distribution as a predictor, constraining the predicted 2021 distribution to areas near existing populations and thus reflecting the limited rhizome-based spread typical of *Sasa*. Comparing the two models allows us to distinguish between the broader potential niche under seed dispersal and the more localized realized expansion expected from clonal growth, providing a realistic range of possible future scenarios.

#### 2.4.1. Explanatory variables

Both models incorporated elevation, slope, aspect, roughness, the Terrain Ruggedness Index (TRI), the Topographic Position Index (TPI), and snowmelt day of year (DOY) as explanatory variables. These topographic features were derived from a 5 m digital elevation model (DEM) provided by the Geospatial Information Authority of Japan and resampled to 1 m resolution to match the vegetation maps.

Snowmelt DOYs were obtained from time-lapse imagery. Although interannual fluctuations were observed, snowmelt timing showed an advancing trend over the past decade. To represent this temporal trend, we fitted a linear regression to per-pixel snowmelt DOYs for each year from 2011 to 2021 and used the predicted 2021 values as explanatory variables in both models. The mean regression coefficient was  $-0.86$ , corresponding to an advance of 8.6 days per decade. For future projections, we extended the same regressions to estimate snowmelt DOYs for 2030 at each pixel. Although some areas obscured by foreground snow cover had uncertain snowmelt dates, these areas showed minimal overlap with the *Sasa* distribution and thus had little impact on our analysis. Additional details on snowmelt timing and its prediction are provided in the supplementary

216 information. In the TDM, distance from the 2012 *Sasa* distribution was included  
217 as an additional explanatory variable to represent dispersal limitation.

#### 218 2.4.2. Target variable

219 The TBM was trained to predict the *Sasa* distribution in 2021. Because many  
220 *Sasa* patches present in 2012 persisted through 2021, pixels located directly  
221 within the 2012 distribution (i.e., at 0 m distance) were excluded from the TDM.  
222 Accordingly, the TDM was designed to predict newly colonized locations that  
223 appeared between 2012 and 2021.

#### 224 2.4.3. Data sampling and splitting

##### 225 2.4.3.1. Data sampling.

226 Because the *Sasa* distribution is relatively limited compared with other vegeta-  
227 tion types (Figure 2), the dataset was imbalanced. To address this, presence  
228 data were retained at 1 m resolution, whereas absence data were downsampled  
229 to 5 m resolution to reduce dominance by non-*Sasa* pixels. Additionally, areas  
230 above 2,560 m—where *Sasa* does not occur—were excluded from the analysis.

##### 231 2.4.3.2. Initial splitting.

232 To evaluate model performance, we divided the dataset into 80% for training  
233 and 20% for testing. Given the strong spatial autocorrelation among explanatory  
234 variables, we applied spatial block splitting using the R packages **spatialsample**  
235 (Mahoney et al., 2023) and **tidysdm** (Leonardi et al., 2024) to mitigate overfitting  
236 effects (Figure 3, left).

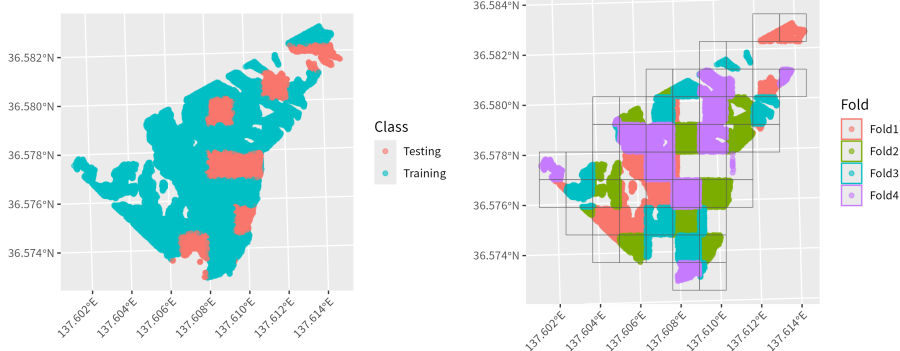


Figure 3: Visualizations of spatial sampling.

The initial split is shown on the left, and the fourfold split used for cross-validation is shown on the right. Spatial sampling was implemented during data splitting to reduce the risk of model overfitting caused by spatial autocorrelation.

##### 237 2.4.3.3. Cross-validation.

238 For hyperparameter tuning and ensemble construction, we performed fourfold  
239 cross-validation using the same spatial block splitting approach (Figure 3, right)  
240 on the training dataset.

241 2.4.4. Model preparation

242 2.4.4.1. Model training and evaluation.

243 We applied four classification algorithms: gradient boosted trees (GBT; Friedman (2001)), maximum entropy (MaxEnt; Phillips et al. (2006)), random forest (RF; Breiman (2001)), and generalized additive models (GAM). For all models except GAM, hyperparameters were tuned via grid search with up to 18 trials.  
244 Model performance was evaluated using the True Skill Statistic (TSS; Allouche et al. (2006); see Equation 1), which ranges from 0 to 1, with higher values  
245 indicating greater predictive accuracy. (TP), (FP), and (FN) denote the numbers  
246 of true positives, false positives, and false negatives, respectively.  
247

$$\begin{aligned} \text{recall} &= \frac{TP}{TP + FN} \\ \text{specificity} &= \frac{TN}{TN + FP} \\ \text{TSS} &= \text{recall} + \text{specificity} - 1 \end{aligned} \quad (1)$$

251 2.4.4.2. Model ensembling.

252 We constructed ensemble models using the `blend_predictions` function in  
253 the R package `stacks` (Couch and Kuhn (2024)), which estimates blending  
254 coefficients via LASSO regularization to maximize cross-validated performance.  
255 The ensemble TSS was subsequently evaluated on the independent test dataset.

256 2.4.4.3. Variable importance computation.

257 For both the TBM and TDM, variable importance was assessed using permutation  
258 loss, defined as the reduction in TSS observed when each explanatory variable  
259 was randomly permuted. This measure quantifies the relative contribution of  
260 each variable to the overall predictive performance of the model.

261 2.4.5. Future prediction and definition of risky areas

262 Using ensemble models built for each of the TBM and TDM, we predicted *Sasa*  
263 distribution for 2030 based on the estimated snowmelt DOYs (see Section 2.4.1).  
264 In this framework, predictions from the TBM represent areas that could become  
265 suitable if *Sasa* disperses via seeds. Under such conditions, *Sasa* is particularly  
266 likely to invade low-height alpine grasslands, which correspond to the “Other  
267 Vegetation” category in our classification. For conservation purposes, we therefore  
268 defined “risky areas” as cells classified as “Other Vegetation” in 2021 whose  
269 TBM-predicted habitat suitability (HS) for 2030 exceeded 0.5, and we extracted  
270 their spatial distribution accordingly.

### 271 3. Results

#### 272 3.1. Changes in *Sasa* distribution between 2012 and 2021

273 The area occupied by *Sasa* increased from 8,542 m<sup>2</sup> in 2012 to 10,170 m<sup>2</sup> in  
274 2021, a net gain of 1,628 m<sup>2</sup> over nine years (+19% relative to 2012). The total

275 expansion area—pixels that transitioned from non-*Sasa* to *Sasa*—amounted to  
 276  $4,095 \text{ m}^2$  (+48% relative to 2012), while the decrease area (from *Sasa* to non-  
 277 *Sasa*) was  $2,467 \text{ m}^2$ . Many of these apparent decreases likely resulted from shrub  
 278 encroachment and growth. Under such conditions, *Sasa* can persist beneath  
 279 shrub canopies but becomes undetectable in time-lapse imagery. Therefore, we  
 280 adopted the expansion area ( $4,095 \text{ m}^2$ ) as the primary metric of change. The  
 281 spatial distribution of expansion is shown in Figure 4. The observed +48%  
 282 increase over nine years is consistent with previous findings from nearby regions  
 283 reporting up to +260% expansion over 38 years (Yoshida et al. (2016)).

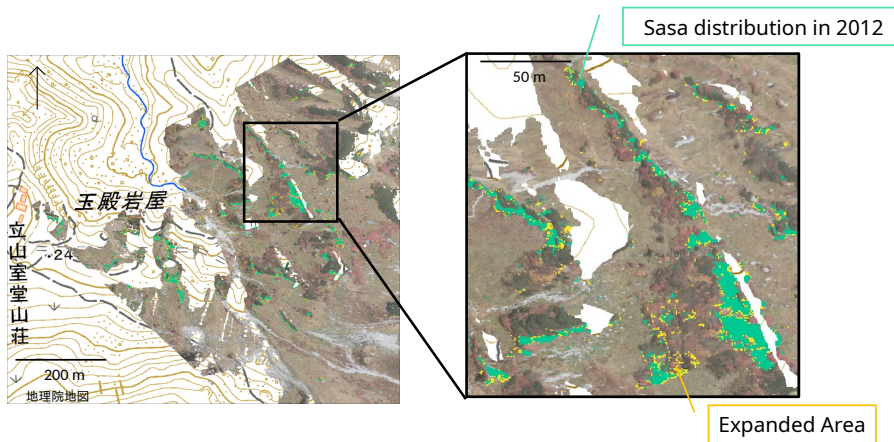


Figure 4: Distribution of *Sasa* expansion between 2012 and 2021.  
 The area occupied by *Sasa* was  $8,542 \text{ m}^2$  in 2012 (shown in green) and expanded by  $4,095 \text{ m}^2$   
 (shown in yellow) by 2021, corresponding to a 48% increase relative to 2012.

### 284 3.2. HSM performance and variable importance

285 The TDM consistently achieved higher TSS values than the TBM. Within  
 286 the TBM, GBT and MaxEnt performed best, while within the TDM, GBT,  
 287 MaxEnt, and RF outperformed GAM. Ensemble TSS on the test dataset was  
 288 0.55 for the TBM and 0.70 for the TDM, indicating clear performance gains  
 289 from incorporating distance in addition to topographic features.

290 Permutation-based variable importance (Figure 6) identified snowmelt DOY  
 291 as the most influential predictor in the TBM, whereas distance from the 2012  
 292 *Sasa* distribution was the strongest predictor in the TDM, followed by snowmelt  
 293 DOY.

294 For the 2021 habitat suitability (HS) maps (Figure 7), the TBM predicted  
 295  $47,253 \text{ m}^2$  of suitable habitat ( $\text{HS} > 0.5$ ), substantially overestimating the  
 296 observed distribution ( $10,170 \text{ m}^2$ ). In contrast, the TDM predicted  $12,766 \text{ m}^2$ ,  
 297 much closer to observations.

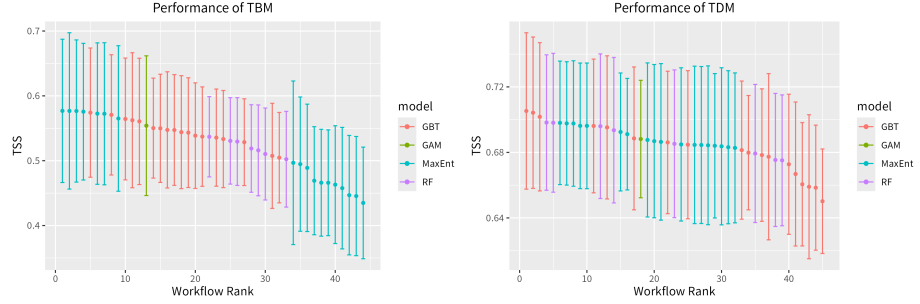


Figure 5: Performance metrics of HSMs obtained through hyperparameter tuning during cross-validation.

TSS scores of HSMs obtained through hyperparameter tuning during cross-validation. The TDM consistently achieved higher TSS values than the TBM, indicating superior predictive performance. Within the TBM framework, GBT and MaxEnt models performed best, whereas within the TDM framework, GBT, MaxEnt, and RF models showed comparably high accuracy.

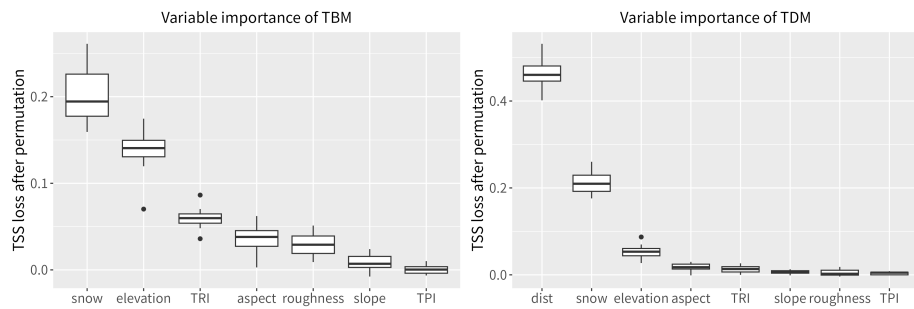


Figure 6: Variable importance for TBM and TDM.

Variable importance based on permutation loss for the TBM and TDM. In the TBM, snowmelt DOY was the most influential variable, whereas in the TDM, distance from the 2012 *Sasa* distribution was the most important, followed by snowmelt DOY.

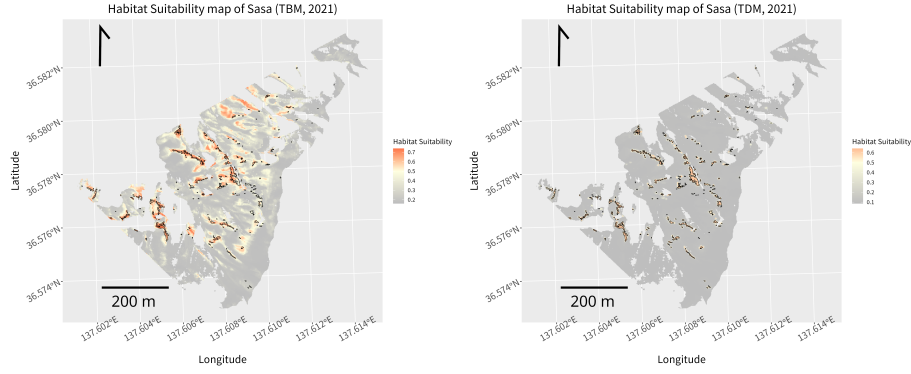


Figure 7: Predicted habitat suitability of *Sasa* in 2021.

Habitat suitability (HS) maps for 2021 generated by the TBM and TDM. The maps show areas predicted as suitable for *Sasa* habitation ( $HS > 0.5$ ). The TBM predicted  $47,253\text{ m}^2$  as suitable, substantially overestimating the observed distribution of  $10,170\text{ m}^2$ . In contrast, the TDM predicted  $12,766\text{ m}^2$ , closely matching the observed distribution and demonstrating higher accuracy in reproducing the actual *Sasa* distribution.

298    3.3. Future prediction and risky areas

299    From the 2030 HS maps and their differences from 2021 (Figure 8), TBM  
300    predicted  $27,049\text{ m}^2$  (57% of the 2021 TBM suitable area) of newly suitable  
301    habitat by 2030, while TDM predicted  $4,387\text{ m}^2$  (34%). Conversely, of the areas  
302    occupied by *Sasa* in 2021, TBM predicted  $2,257\text{ m}^2$  (21%) to become unsuitable  
303    by 2030, and TDM predicted  $717\text{ m}^2$  (7%) to become unsuitable.

304    The spatial distribution of risky areas—cells classified as “Other Vegetation”  
305    in 2021 with TBM HS  $> 0.5$  in 2030—is shown in Figure 9.

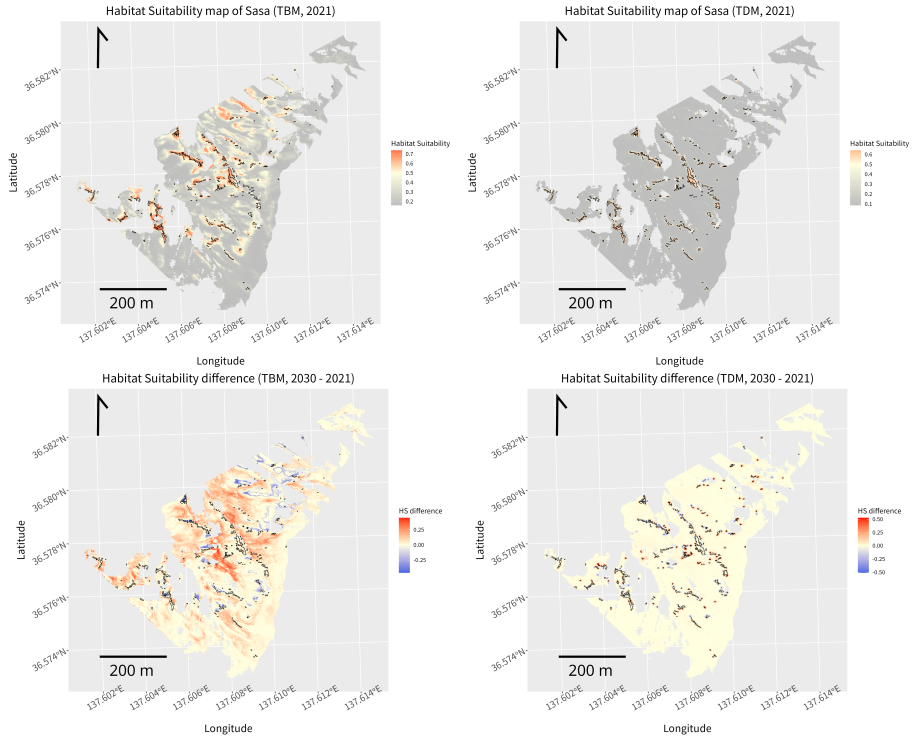


Figure 8: Predicted habitat suitability of Sasa in 2030 and differences from 2021.

Habitat suitability (HS) maps for 2030 and differences from the 2021 HS maps. The TBM predicted  $27,049 \text{ m}^2$  (57% of the 2021 suitable area) as newly suitable for Sasa in 2030, while the TDM predicted  $4,387 \text{ m}^2$  (34%) as newly suitable. These projections indicate a potential Sasa distribution expansion similar to the past decade. Additionally, even in areas where Sasa was present in 2021, some regions are expected to become unsuitable by 2030. The TBM identifies  $2,257 \text{ m}^2$  (21%) as unsuitable, while the TDM identifies  $717 \text{ m}^2$  (7%) as unsuitable. These reductions suggest shifts in habitat suitability and Sasa distribution due to earlier snowmelt timing.

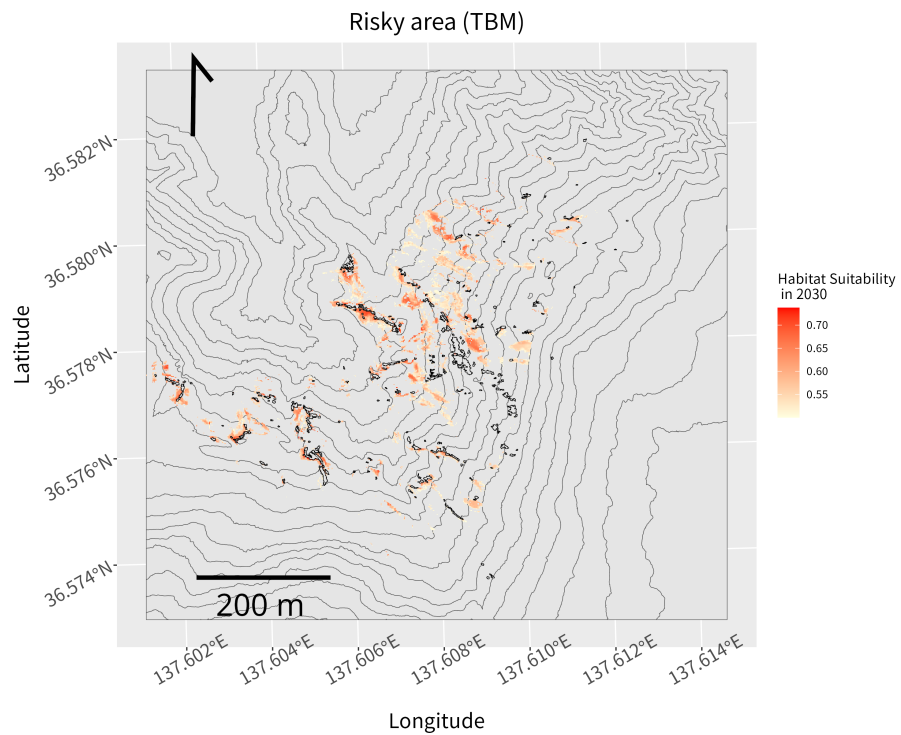


Figure 9: Predicted potential habitats for *Sasa* (risky areas). Potential habitats were extracted from the TBM predictions to support future monitoring and conservation planning. “Risky areas” were defined as cells classified as “Other Vegetation” in 2021 with a predicted 2030 habitat suitability (HS) greater than 0.5.

306    **4. Discussion**

307    This study demonstrates how snowmelt-driven processes can be quantified and  
308    projected at fine spatial scales using ground-based time-lapse imagery integrated  
309    with habitat suitability models (HSMs). Using a Japanese alpine system as  
310    a model case, we assessed recent changes and potential future expansion of a  
311    competitively dominant plant (*Sasa*) at an exceptionally high spatial resolution  
312    (1 m). Beyond documenting local vegetation change, our results highlight how  
313    snowmelt timing acts as a key biogeographic driver structuring alpine vegetation  
314    patterns and dynamics.

315    *4.1. Snowmelt timing as a driver of dominant plant expansion*

316    Comparison of vegetation classification maps from 2012 and 2021 enabled us to  
317    spatially identify areas of *Sasa* expansion. Incorporating HSMs further allowed  
318    us to investigate the environmental factors driving this expansion. Variable  
319    importance analyses for both the TBM and TDM (Figure 6) indicated that  
320    snowmelt DOY was a major determinant. Moreover, predictions for 2030,  
321    assuming earlier snowmelt than in 2021, suggested continued *Sasa* expansion.  
322    These results indicate that earlier snowmelt has facilitated the expansion of a  
323    competitively dominant plant, consistent with previous findings (Kudo et al.  
324    (2011)) linking earlier snowmelt to increased soil dryness and extended growing  
325    periods that favor *Sasa* growth.

326    At the same time, the TBM substantially overestimated *Sasa* distribution in  
327    2021. Although adding distance as an explanatory variable improved model  
328    accuracy, at least two interpretations of the overestimation are possible. First,  
329    areas predicted as suitable by the TBM may indeed be habitable, but *Sasa* has not  
330    yet colonized them due to its limited dispersal capacity. In fact, no isolated *Sasa*  
331    patches formed by seed dispersal were observed in the expansion areas between  
332    2012 and 2021, supporting the idea that low dispersal ability creates a large gap  
333    between potential and realized niches. Second, the overestimation may reflect  
334    missing explanatory variables. In this case, *Sasa* generally occupies its potential  
335    niche, but the TBM overestimated distribution because it failed to incorporate  
336    important environmental factors. The improved accuracy of the TDM could then  
337    be explained by a strong spatial correlation between the 2012 distribution and  
338    such unmeasured variables. Soil structure or soil moisture, for instance, could play  
339    this role. To distinguish between these interpretations, the TBM should ideally  
340    be extended to include additional environmental predictors, although obtaining  
341    such comprehensive datasets remains challenging. Alternatively, process-based  
342    models that explicitly simulate dispersal dynamics could help clarify whether  
343    the overestimation results from dispersal limitation or omitted environmental  
344    factors.

345    *4.2. Methodological implications for conservation biogeography*

346    This study demonstrates that combining time-lapse cameras with HSMs enables  
347    exceptionally fine-scale (1 m) prediction of vegetation distribution changes driven

348 by climate-related processes. The integration of time-lapse imagery and HSMs  
349 is unprecedented. In contrast, conventional species distribution models typically  
350 operate at much coarser resolutions (e.g., 1 km), as future climate projections  
351 are generally available only at coarse spatial scales (e.g., alpine vegetation  
352 studies: [Amagai et al. \(2022\)](#)). By directly observing snowmelt timing—a  
353 key determinant of alpine vegetation dynamics—using time-lapse cameras, we  
354 achieved high-resolution predictions that would be difficult to obtain using  
355 satellite-based or plot-based approaches alone.

356 Because snowmelt timing requires both frequent and spatially extensive mon-  
357 itoring, time-lapse cameras are particularly well suited for capturing this bio-  
358 geographic driver. This approach provides a pathway for linking climate-driven  
359 processes to spatial vegetation patterns in alpine and other snow-dominated  
360 ecosystems where conventional monitoring methods are limited.

#### 361 *4.3. Future projections and scenario-based interpretation*

362 In this study, future snowmelt timing was predicted using a simple linear  
363 regression based on a decade of past observations. While this approach provided  
364 a useful proof of concept, it does not represent a realistic long-term forecast. In  
365 alpine regions, strong seasonal winds and complex topography cause substantial  
366 snow redistribution, making accurate snowmelt prediction a persistent challenge.  
367 Accordingly, the future *Sasa* expansion presented here should be interpreted  
368 not as a literal forecast but as a scenario based on the assumption of continued  
369 earlier snowmelt. As high-resolution climate and snow models improve, this  
370 framework can readily incorporate more realistic projections, thereby refining  
371 predictions of vegetation redistribution.

#### 372 *4.4. Conservation implications*

373 The expansion of competitively dominant species such as *Sasa* poses a serious  
374 threat to alpine biodiversity by reducing habitat availability for subordinate and  
375 often rare alpine plants. High-resolution predictions of vegetation change, as  
376 demonstrated here, provide a practical basis for conservation management by  
377 identifying priority areas for intervention, such as targeted *Sasa* removal, and  
378 for designing efficient long-term monitoring strategies. More broadly, our results  
379 emphasize that snowmelt timing is a critical process shaping alpine vegetation  
380 patterns and that fine-scale, process-based monitoring can substantially enhance  
381 conservation planning in climate-sensitive mountain ecosystems.

### 382 **5. Conclusion**

383 This study demonstrated the effectiveness of integrating time-lapse cameras with  
384 habitat suitability models (HSMs) to detect and predict changes in vegetation  
385 distribution at 1 m resolution. Focusing on the expansion of *Sasa* in the northern  
386 Japanese Alps, we quantified its distributional changes over the past nine years  
387 and identified earlier snowmelt as a major driver of its spread. Furthermore,

<sup>388</sup> our projections indicate that *Sasa* expansion is likely to continue in the coming  
<sup>389</sup> decades.

<sup>390</sup> The expansion of *Sasa* poses a serious threat to alpine plant diversity, and the  
<sup>391</sup> framework developed here provides direct applications for conservation planning.  
<sup>392</sup> Predictions at 1 m resolution offer practical guidance for selecting monitoring  
<sup>393</sup> sites and prioritizing areas for *Sasa* removal, enabling more efficient allocation  
<sup>394</sup> of conservation resources. Beyond *Sasa*, this approach can be extended to other  
<sup>395</sup> invasive species, as well as to plant communities highly sensitive to climate change,  
<sup>396</sup> demonstrating broad potential for use in alpine regions and other vulnerable  
<sup>397</sup> ecosystems worldwide.

<sup>398</sup> In summary, this study highlights the power of combining high-frequency time-  
<sup>399</sup> lapse observations with HSM-based modeling to advance the understanding and  
<sup>400</sup> prediction of vegetation dynamics. This integrated framework refines climate  
<sup>401</sup> impact assessment in alpine ecosystems and supports the development of practical,  
<sup>402</sup> conservation-oriented ecology.

403     **6. Data Availability Statement**

404     The data and scripts supporting this study are openly available in an anonymous  
405     public repository for peer review at: [https://anonymous.4open.science/r/  
406     SasaSDMPaper-67CE/](https://anonymous.4open.science/r/SasaSDMPaper-67CE/)

407     **References**

- 408     Allouche, O., Tsoar, A., Kadmon, R., 2006. Assessing the accuracy of  
409     species distribution models: prevalence, kappa and the true skill statistic  
410     (tss). Journal of Applied Ecology 43, 1223–1232. URL: <https://onlinelibrary.wiley.com/doi/full/10.1111/j.1365-2664.2006.01214.x>  
411     <https://onlinelibrary.wiley.com/doi/abs/10.1111/j.1365-2664.2006.01214.x>  
412     <https://besjournals.onlinelibrary.wiley.com/doi/10.1111/j.1365-2664.2006.01214.x>,  
413     doi:[10.1111/j.1365-2664.2006.01214.X](https://doi.org/10.1111/j.1365-2664.2006.01214.x).
- 415     Amagai, Y., Oguma, H., Ishihama, F., 2022. Predicted scarcity of  
416     suitable habitat for alpine plant communities in northern japan  
417     under climate change. Applied Vegetation Science , e12694URL:  
418     <https://onlinelibrary.wiley.com/doi/full/10.1111/avsc.12694>  
419     <https://onlinelibrary.wiley.com/doi/abs/10.1111/avsc.12694>  
420     <https://wiley.com/doi/10.1111/avsc.12694>, doi:[10.1111/AVSC.12694](https://doi.org/10.1111/AVSC.12694).
- 421     Bakkenes, M., Alkemade, J.R., Ihle, F., Leemans, R., Latour, J.B., 2002. Assessing effects of forecasted climate change on the diversity and distribution of european higher plants for 2050. Global Change Biology 8, 390–407. URL: <https://onlinelibrary.wiley.com/doi/full/10.1046/j.1354-1013.2001.00467.x>  
422     <https://onlinelibrary.wiley.com/doi/abs/10.1046/j.1354-1013.2001.00467.x>  
423     <https://onlinelibrary.wiley.com/doi/10.1046/j.1354-1013.2001.00467.x>, doi:[10.1046/j.1354-1013.2001.00467.X](https://doi.org/10.1046/j.1354-1013.2001.00467.x).
- 428     Breiman, L., 2001. Random forests. Machine Learning 45, 5–32. URL:  
429     <https://link.springer.com/article/10.1023/A:1010933404324>, doi:[10.1023/A:1010933404324/METRICS](https://doi.org/10.1023/A:1010933404324/METRICS).
- 431     Couch, S., Kuhn, M., 2024. Tidy model stacking [r package stacks version 1.0.5].  
432     CRAN: Contributed Packages URL: <https://CRAN.R-project.org/package=stacks>, doi:[10.32614/CRAN.PACKAGE.STACKS](https://doi.org/10.32614/CRAN.PACKAGE.STACKS).
- 434     Dullinger, S., Dirnböck, T., Grabherr, G., 2003. Patterns of shrub invasion into  
435     high mountain grasslands of the northern calcareous alps, austria. Arctic,  
436     Antarctic, and Alpine Research 35, 434–441. URL: <http://www.jstor.org/stable/1552344>.
- 438     Friedman, J.H., 2001. Greedy function approximation: A gradient boosting  
439     machine. The Annals of Statistics 29, 1189–1232. URL: <https://doi.org/10.1214/aos/1013203451>, doi:[10.1214/aos/1013203451](https://doi.org/10.1214/aos/1013203451).

- 441 Gallien, L., Douzet, R., Pratte, S., Zimmermann, N.E., Thuiller, W., 2012.  
442 Invasive species distribution models – how violating the equilibrium assumption  
443 can create new insights. *Global Ecology and Biogeography* 21, 1126–1136.  
444 URL: <https://doi.org/10.1111/j.1466-8238.2012.00768.x>, doi:<https://doi.org/10.1111/j.1466-8238.2012.00768.x>.
- 446 Gallien, L., Münkemüller, T., Albert, C.H., Boulangeat, I., Thuiller, W.,  
447 2010. Predicting potential distributions of invasive species: where to  
448 go from here? *Diversity and Distributions* 16, 331–342. URL: <https://onlinelibrary.wiley.com/doi/full/10.1111/j.1472-4642.2010.00652.x>  
449 <https://onlinelibrary.wiley.com/doi/abs/10.1111/j.1472-4642.2010.00652.x>  
450 <https://onlinelibrary.wiley.com/doi/10.1111/j.1472-4642.2010.00652.x>,  
451 doi:[10.1111/j.1472-4642.2010.00652.x](https://doi.org/10.1111/j.1472-4642.2010.00652.x).
- 453 Gottfried, M., Pauli, H., Futschik, A., Akhalkatsi, M., Barančok, P., Alonso,  
454 J.L.B., Coldea, G., Dick, J., Erschbamer, B., Calzado, M.R.F., Kazakis, G.,  
455 Krajčí, J., Larsson, P., Mallaun, M., Michelsen, O., Moiseev, D., Moiseev, P.,  
456 Molau, U., Merzouki, A., Nagy, L., Nakhutsrishvili, G., Pedersen, B., Pelino,  
457 G., Puscas, M., Rossi, G., Stanisci, A., Theurillat, J.P., Tomaselli, M., Villar,  
458 L., Vittoz, P., Vogiatzakis, I., Grabherr, G., 2012. Continent-wide response of  
459 mountain vegetation to climate change. *Nature Climate Change* 2, 111–115.  
460 URL: [www.nature.com/natureclimatechange](http://www.nature.com/natureclimatechange), doi:[10.1038/nclimate1329](https://doi.org/10.1038/nclimate1329).
- 461 Grabherr, G., 2003. Alpine Vegetation Dynamics and Climate Change - a  
462 Synthesis of Long-Term Studies and Observations. Springer Berlin Heidelberg.  
463 pp. 399–409. URL: [https://doi.org/10.1007/978-3-642-18967-8\\_24](https://doi.org/10.1007/978-3-642-18967-8_24), doi:[10.1007/978-3-642-18967-8\24](https://doi.org/10.1007/978-3-642-18967-8\24).
- 465 Grabherr, G., Gottfried, M., Pauli, H., 2010. Climate change impacts in  
466 alpine environments. *Geography Compass* 4, 1133–1153. URL: <https://onlinelibrary.wiley.com/doi/full/10.1111/j.1749-8198.2010.00356.x>  
467 <https://onlinelibrary.wiley.com/doi/abs/10.1111/j.1749-8198.2010.00356.x>  
468 <https://compass.onlinelibrary.wiley.com/doi/10.1111/j.1749-8198.2010.00356.x>,  
469 doi:[10.1111/j.1749-8198.2010.00356.x](https://doi.org/10.1111/j.1749-8198.2010.00356.x).
- 471 Guisan, A., Theurillat, J., Kienast, F., 1998. Predicting the potential distribution  
472 of plant species in an alpine environment. *Journal of Vegetation Science* 9,  
473 65–74. doi:[10.2307/3237224](https://doi.org/10.2307/3237224).
- 474 Hock, R., Rasul, G., Adler, C., Ca;ceres, B., Gruber, S., Hirabayashi, Y., Jackson,  
475 M., Kääb, A., Kang, S., Kutuzov, S., Milner, A., Molau, U., Morin, S., Orlove,  
476 B., Steltzer, H., Allen, S., Arenson, L., Banerjee, S., Barr, I., Bórquez, R.,  
477 Brown, L., Cao, B., Carey, M., Cogley, G., Fischlin, A., de Sherbinin, A.,  
478 Eckert, N., Geertsema, M., Hagenstad, M., Honsberg, M., Hood, E., Huss,  
479 M., Zamora, E.J., Kotlarski, S., Lefevre, P.M., Moreno, J.I.L., Lundquist,  
480 J., McDowell, G., Mills, S., Mou, C., Nepal, S., Noetzli, J., Palazzi, E.,  
481 Pepin, N., Rixen, C., Shahgedanova, M., Skiles, S.M., Vincent, C., Vivioli,  
482 D., Weyhenmeyer, G.A., Sherpa, P.Y., Weyen, N., Wouters, B., Yasunari,

- 483 T., You, Q., Zhang, Y., 2019. High Mountain Areas. Cambridge University  
484 Press. pp. 131–202. URL: <https://www.ipcc.ch/srocc/chapter/chapter-2/>,  
485 doi:[10.1017/9781009157964.004](https://doi.org/10.1017/9781009157964.004).
- 486 Ide, R., Oguma, H., 2013. A cost-effective monitoring method using digital  
487 time-lapse cameras for detecting temporal and spatial variations of snowmelt  
488 and vegetation phenology in alpine ecosystems. Ecological Informatics 16,  
489 25–34. URL: <https://doi.org/10.1016/j.ecoinf.2013.04.003>, doi:[10.1016/J.ECOINF.2013.04.003](https://doi.org/10.1016/J.ECOINF.2013.04.003).
- 490 Klanderud, K., 2005. Climate change effects on species interactions in an  
491 alpine plant community. Journal of Ecology 93, 127–137. URL: <https://onlinelibrary.wiley.com/doi/full/10.1111/j.1365-2745.2004.00944.x>  
492 <https://onlinelibrary.wiley.com/doi/abs/10.1111/j.1365-2745.2004.00944.x>  
493 <https://besjournals.onlinelibrary.wiley.com/doi/10.1111/j.1365-2745.2004.00944.x>,  
494 doi:[10.1111/J.1365-2745.2004.00944.X](https://doi.org/10.1111/J.1365-2745.2004.00944.X).
- 495 Kudo, G., Amagai, Y., Hoshino, B., Kaneko, M., 2011. Invasion of  
496 dwarf bamboo into alpine snow-meadows in northern japan: pattern of  
497 expansion and impact on species diversity. Ecology and Evolution 1,  
498 85–96. URL: <https://onlinelibrary.wiley.com/doi/full/10.1002/ece3.9>  
499 <https://onlinelibrary.wiley.com/doi/abs/10.1002/ece3.9>  
500 <https://onlinelibrary.wiley.com/doi/10.1002/ece3.9>, doi:[10.1002/ECE3.9](https://doi.org/10.1002/ECE3.9).
- 501 Kudo, G., Kawai, Y., Amagai, Y., Winkler, D.E., 2017. Degradation and recovery  
502 of an alpine plant community: experimental removal of an encroaching dwarf  
503 bamboo. Alpine Botany 127, 75–83. URL: <https://link.springer.com/article/10.1007/s00035-016-0178-2>, doi:[10.1007/S00035-016-0178-2](https://doi.org/10.1007/S00035-016-0178-2).
- 504 Larson, M.A., Thompson, F.R., Millspaugh, J.J., Dijak, W.D., Shifley, S.R., 2004.  
505 Linking population viability, habitat suitability, and landscape simulation  
506 models for conservation planning. Ecological Modelling 180, 103–118. doi:[10.1016/J.ECOLMODEL.2003.12.054](https://doi.org/10.1016/J.ECOLMODEL.2003.12.054).
- 507 Leonardi, M., Colucci, M., Pozzi, A.V., Scerri, E.M., Manica, A., 2024.  
508 tidysdm: Leveraging the flexibility of tidyverse for species distribution  
509 modelling in r. Methods in Ecology and Evolution 15, 1789–1795. URL:  
510 <https://onlinelibrary.wiley.com/doi/full/10.1111/2041-210X.14406>  
511 <https://onlinelibrary.wiley.com/doi/abs/10.1111/2041-210X.14406>  
512 <https://besjournals.onlinelibrary.wiley.com/doi/10.1111/2041-210X.14406>,  
513 doi:[10.1111/2041-210X.14406](https://doi.org/10.1111/2041-210X.14406).
- 514 Mahoney, M.J., Johnson, L.K., Silge, J., Frick, H., Kuhn, M., Beier, C.M., 2023.  
515 Assessing the performance of spatial cross-validation approaches for models of  
516 spatially structured data URL: <https://arxiv.org/abs/2303.07334v1>.
- 517 Miyazaki, Y., Ohnishi, N., Takafumi, H., Hiura, T., 2009. Genets of dwarf  
518 bamboo do not die after one flowering event: Evidence from genetic structure  
519 and flowering pattern. Journal of Plant Research 122, 523–528. URL: <https://doi.org/10.1007/s10261-009-0523-0>.

- 524            //link.springer.com/article/10.1007/s10265-009-0241-9, doi:10.1007/S10265-  
 525            009-0241-9/TABLES/1.
- 526 Mizuki, I., Sato, A., Matsuo, A., Suyama, Y., Suzuki, J.I., Makita, A., 2014.  
 527            Clonal structure, seed set, and self-pollination rate in mass-flowering bamboo  
 528            species during off-year flowering events. PLOS ONE 9, e105051. URL: <https://journals.plos.org/plosone/article?id=10.1371/journal.pone.0105051>, doi:10.  
 529            1371/JOURNAL.PONE.0105051.
- 530            Okamoto, R., Ide, R., Oguma, H., 2024. Automatically drawing vegetation  
 531            classification maps using digital time-lapse cameras in alpine  
 532            ecosystems. Remote Sensing in Ecology and Conservation 10, 188–202.  
 533            URL: <https://onlinelibrary.wiley.com/doi/full/10.1002/rse2.364><https://zslpublications.onlinelibrary.wiley.com/doi/10.1002/rse2.364>, doi:10.1002/RSE2.364.
- 534            Otsu, N., 1979. A threshold selection method from gray-level histograms. IEEE  
 535            Trans Syst Man Cybern SMC-9, 62–66. doi:10.1109/TSMC.1979.4310076.
- 536            Phillips, S.B., Aneja, V.P., Kang, D., Arya, S.P., 2006. Maximum entropy modeling of species geographic distributions. Ecological Modelling 190, 231–259.  
 537            doi:10.1016/J.ECOLMODEL.2005.03.026.
- 538            Portenier, C., Hüsler, F., Härer, S., Wunderle, S., 2020. Towards a webcam-based  
 539            snow cover monitoring network: Methodology and evaluation. Cryosphere 14,  
 540            1409–1423. doi:10.5194/TC-14-1409-2020.
- 541            Suyama, Y., Obayashi, K., Hayashi, I., 2000. Clonal structure in a  
 542            dwarf bamboo (*sasa senanensis*) population inferred from amplified  
 543            fragment length polymorphism (aflp) fingerprints. Molecular Ecology 9,  
 544            901–906. URL: <https://onlinelibrary.wiley.com/doi/full/10.1046/j.1365-294x.2000.00943.x><https://onlinelibrary.wiley.com/doi/abs/10.1046/j.1365-294x.2000.00943.x><https://onlinelibrary.wiley.com/doi/10.1046/j.1365-294x.2000.00943.x>, doi:10.1046/J.1365-294X.2000.00943.X.
- 545            Thomas, C.D., Cameron, A., Green, R.E., Bakkenes, M., Beaumont, L.J.,  
 546            Collingham, Y.C., Erasmus, B.F., Siqueira, M.F.D., Grainger, A., Hannah,  
 547            L., Hughes, L., Huntley, B., Jaarsveld, A.S.V., Midgley, G.F., Miles, L.,  
 548            Ortega-Huerta, M.A., Peterson, A.T., Phillips, O.L., Williams, S.E., 2004.  
 549            Extinction risk from climate change. Nature 2003 427:6970 427, 145–148. URL:  
 550            <https://www.nature.com/articles/nature02121>, doi:10.1038/nature02121.
- 551            Xue, T., Gadagkar, S.R., Albright, T.P., Yang, X., Li, J., Xia, C., Wu, J., Yu, S.,  
 552            2021. Prioritizing conservation of biodiversity in an alpine region: Distribution  
 553            pattern and conservation status of seed plants in the qinghai-tibetan plateau.  
 554            Global Ecology and Conservation 32, e01885. doi:10.1016/J.GECCO.2021.  
 555            E01885.

563 Yoshida, M., Takahashi, K., Ohmiya, T., 2016. Expansion of dwarf bamboo  
564 communities in murodo-daira, tateyama mountains, as revealed by aerial  
565 photography. Bulletin of the Botanic Gardens of Toyama , 9–17.